CADO: From Imitation to Cost Minimization for Heatmap-based Solvers in Combinatorial Optimization

Anonymous authors
Paper under double-blind review

Abstract

Heatmap-based solvers have emerged as a promising paradigm for Combinatorial Optimization (CO). However, we argue that the dominant Supervised Learning (SL) training paradigm suffers from a fundamental objective mismatch: minimizing imitation loss (e.g., cross-entropy) does not guarantee solution cost minimization. We dissect this mismatch into two deficiencies: Decoder-Blindness (being oblivious to the non-differentiable decoding process) and Cost-Blindness (prioritizing structural imitation over solution quality). We empirically demonstrate that these intrinsic flaws impose a hard performance ceiling. To overcome this limitation, we propose CADO (**C**ost-**A**ware **D**iffusion models for **O**ptimization), a streamlined Reinforcement Learning fine-tuning framework that formulates the diffusion denoising process as an MDP to directly optimize the post-decoded solution cost. We introduce Label-Centered Reward, which repurposes ground-truth labels as unbiased baselines rather than imitation targets, and Hybrid Fine-Tuning for parameter-efficient adaptation. CADO achieves state-of-the-art performance across diverse benchmarks, validating that objective alignment is essential for unlocking the full potential of heatmap-based solvers.

1 Introduction

Combinatorial optimization (CO) problems are notoriously challenging owing to their inherent NP-hardness (Karp, 1975). Neural Combinatorial Optimization (NCO) has emerged as a promising alternative to traditional heuristics (Lin & Kernighan, 1973; Helsgaun, 2017) and exact solvers (Applegate et al., 2006; Vielma, 2015). While **autoregressive solvers**—which iteratively construct solutions by extending partial candidates—have dominated the field with their strong performance (Kool et al., 2019; da Costa et al., 2020; Kwon et al., 2020; Wu et al., 2022; Kim et al., 2022), **heatmap-based solvers** have recently shown significant promise due to their expressive power in modeling high-dimensional distributions and capability for efficient parallel inference (Joshi et al., 2019; Fu et al., 2021; Geisler et al., 2022). Instead of sequential generation, heatmap-based solvers produce a complete solution probability map (heatmap) in a one-shot manner, which is subsequently discretized into a feasible solution via a lightweight decoding heuristic.

The dominant paradigm for heatmap-based solvers—exemplified by state-of-the-art diffusion models like DIFUSCO (Sun & Yang, 2023)—is **Supervised Learning (SL)**. This approach trains models to generate heatmaps that imitate optimal solutions via surrogate losses (e.g., cross-entropy), treating ground-truth solutions as labels. Although **Reinforcement Learning (RL)** naturally aligns with the true CO objective of cost minimization, SL is generally preferred for its training stability and the tacit assumption that heatmaps approximating optimal solutions will be decoded into low-cost solutions.

However, we challenge this premise. While prior works (Xia et al., 2024) noted the mathematical discrepancy between SL and RL objectives, its actual impact on heatmap solver performance has remained unexplored. We substantiate this theoretical concern by providing the first direct evidence that this objective mismatch leads to substantial performance degradation, empirically demonstrating that closer imitation of optimal solutions does not guarantee lower solution cost (see Figure 3). We identify the SL objective's **Decoder-Blindness** (ignoring the decoding heuristic) and **Cost-Blindness** (neglecting the solution cost) as the twin factors behind this degradation.

To resolve this mismatch, we propose an RL fine-tuning framework for SL-based heatmap solvers designed to optimize the post-decoded solution cost, thereby directly overcoming both Decoder-Blindness and Cost-Blindness. We instantiate this framework on diffusion models as CADO (Cost-Aware Diffusion Models for Optimization), which formulates the denoising process as a Markov Decision Process (MDP). Furthermore, we introduce Label-Centered Reward (LCR), which repurposes SL dataset labels as unbiased baselines rather than imitation targets, and Hybrid Fine-Tuning (Hybrid-FT) for stable and efficient RL fine-tuning.

Our contributions are threefold:

- **Rigorous Analysis of Objective Mismatch.** We empirically identify and dissect the objective mismatch of SL-based heatmap solvers into **Decoder-Blindness** and **Cost-Blindness**, providing the first direct evidence that this mismatch significantly degrades performance.
- **CADO Framework.** We propose CADO, a streamlined RL fine-tuning framework for SL-based heatmap solvers that resolves both blindnesses by explicitly minimizing the post-decoded solution cost, thereby aligning the diffusion process with the true CO objective.
- **Stability and State-of-the-Art Performance.** We introduce Label-Centered Reward (LCR) and Hybrid Fine-Tuning (Hybrid-FT) to stabilize RL training. Extensive experiments demonstrate that CADO consistently outperforms existing baselines across diverse CO benchmarks.

2 Preliminaries

2.1 Problem Formulation

A Combinatorial Optimization (CO) problem instance is denoted by $g \in \mathcal{G}$, where $\mathcal{G}$ is the set of all instances. For each instance g, the problem is defined over a discrete solution space $\mathcal{X}_g$, typically represented as $\{0,1\}^{N_g}$. We define the *feasible solution space* $\mathcal{F}_g \subseteq \mathcal{X}_g$ as the set of solutions that satisfy all instance-specific constraints. The task is then to find a solution $\boldsymbol{x} \in \mathcal{F}_g$ that minimizes the cost function $c_g : \mathcal{F}_g \to \mathbb{R}$, defined as:

$$\boldsymbol{x}^\star = \arg\min_{\boldsymbol{x}\in\mathcal{F}_g} c_g(\boldsymbol{x}). \tag{1}$$

Since most CO problems are NP-hard, finding the exact optimal solution $\boldsymbol{x}^\star$ is computationally intractable. The practical goal is thus to efficiently find a near-optimal solution within a given computational budget. Neural Combinatorial Optimization (NCO) addresses this by learning a (possibly stochastic) policy $\pi_\theta(\boldsymbol{x}|g)$ that models the distribution of feasible solutions $\boldsymbol{x} \in \mathcal{F}_g$ for a given instance g. The learning objective is to determine the optimal parameters $\theta^\star$ that minimize the expected cost over the distribution of instances:

$$\theta^\star = \arg\min_{\theta} \mathbb{E}_{g\sim\mathcal{G}}\left[\mathbb{E}_{\boldsymbol{x}\sim\pi_\theta(\cdot|g)}[c_g(\boldsymbol{x})]\right]. \tag{2}$$

We describe two specific CO problems as examples: the Traveling Salesman Problem (TSP) and the Maximum Independent Set (MIS) problem. In the TSP, an instance g represents the coordinates of n cities to be visited. A feasible solution $\boldsymbol{x}$ is an $n \times n$ matrix, where $\boldsymbol{x}[i,j] = 1$ if the traveler moves from city i to city j and 0 otherwise. The total solution space is $\mathcal{X}_g = \{0,1\}^{n\times n}$, and the feasible solution space $\mathcal{F}_g$ is the set of all valid TSP tours that visit each city exactly once. The cost function $c_g(\cdot)$ represents the total length of the tour. In the Maximum Independent Set (MIS) problem, an instance g represents a graph (V_g, E_g), where V_g and E_g denote the sets of vertices and edges, respectively. The solution space $\mathcal{X}_g = \{0,1\}^{|V_g|}$ indicates whether each vertex $v \in V_g$ is included in the independent set. To satisfy the independence property, a feasible solution $\boldsymbol{x} \in \mathcal{F}_g$ must not contain any two vertices connected by an edge in E_g. To remain consistent with the minimization objective, the cost function $c_g(\cdot)$ is defined as the negative of the total number of selected nodes.

2.2 Neural Combinatorial Optimization Solver

Neural approaches to CO generally fall into two main categories: autoregressive and heatmap-based solvers. **Autoregressive solvers** construct solutions iteratively by extending partial candidates.

Conversely, **heatmap-based solvers** aim to generate a complete feasible solution $\boldsymbol{x} \in \mathcal{F}_g$ in a single forward pass. Since strictly enforcing hard constraints directly within the network output is challenging, this paradigm employs a two-stage decomposition. First, a **heatmap generator** $\tilde{\pi}_\theta : \mathcal{G} \to [0,1]^{N_g}$ maps an instance g to a probabilistic heatmap $\tilde{\boldsymbol{x}} = \tilde{\pi}_\theta(g)$. Subsequently, a **post-processing decoder** $f_g : [0,1]^{N_g} \to \mathcal{F}_g$ projects $\tilde{\boldsymbol{x}}$ into a discrete solution $\boldsymbol{x} \in \mathcal{F}_g$, typically using a lightweight non-differentiable heuristic. The resulting policy $\pi_\theta(\boldsymbol{x}|g)$ is defined by marginalizing over the heatmap $\tilde{\boldsymbol{x}}$:

$$\pi_\theta(\boldsymbol{x}|g) = \int f_g(\boldsymbol{x}|\tilde{\boldsymbol{x}})\tilde{\pi}_\theta(\tilde{\boldsymbol{x}}|g)d\tilde{\boldsymbol{x}}. \tag{3}$$

The training procedure optimizes $\tilde{\pi}_\theta$ while keeping the decoder f_g fixed, using either SL or RL objectives.

The **SL objective** leverages a dataset of optimal solutions $\boldsymbol{x}_g^\star$ as labels. Fundamentally, this approach aims to induce the model to generate solutions structurally close to $\boldsymbol{x}_g^\star$. However, the non-differentiable nature of f_g precludes direct likelihood optimization. Instead, models minimize a surrogate objective, training the generator $\tilde{\pi}_\theta$ to approximate the labels (i.e., $\tilde{\boldsymbol{x}} \approx \boldsymbol{x}_g^\star$) via an instance-level loss $\mathcal{L}_{SL}$ (e.g., cross-entropy):

$$\mathcal{L}(\theta) = \mathbb{E}_{g\sim\mathcal{G},\, \tilde{\boldsymbol{x}}\sim\tilde{\pi}_\theta(\cdot|g)}\left[\mathcal{L}_{SL}(\tilde{\boldsymbol{x}}, \boldsymbol{x}_g^\star)\right]. \tag{4}$$

For the **RL objective**, models operate without labels, directly minimizing the cost of the decoded solution. The generator $\tilde{\pi}_\theta$ is trained to minimize the expectation of the cost $c_g(f_g(\tilde{\boldsymbol{x}}))$ subsequent to decoding via f_g:

$$\mathcal{R}(\theta) = \mathbb{E}_{g\sim\mathcal{G},\, \tilde{\boldsymbol{x}}\sim\tilde{\pi}_\theta(\cdot|g)}\left[-c_g(f_g(\tilde{\boldsymbol{x}}))\right]. \tag{5}$$

Notably, the RL objective $\mathcal{R}(\theta)$ directly optimizes the NCO goal of cost minimization outlined in (2). However, it often suffers from training instability, particularly in large-scale CO problems involving high-dimensional heatmaps. Conversely, while the SL objective $\mathcal{L}(\theta)$ serves as a surrogate, it has been widely regarded as theoretically sound; in principle, if $\tilde{\pi}_\theta$ perfectly imitates the optimal labels, it inherently fulfills the fundamental CO goal as defined in (1). Driven by this theoretical rationale and its superior training stability, the SL paradigm has generally been preferred over RL for heatmap-based solvers.

2.3 Diffusion Models for Combinatorial Optimization

Discrete diffusion models have emerged as a powerful class of generative models (Austin et al., 2021), recently achieving state-of-the-art results among heatmap-based solvers for CO problems (Sun & Yang, 2023). Since these models are trained to mimic the distribution of a given solution dataset by minimizing the SL objective $\mathcal{L}(\theta)$ defined in (4), they are fundamentally classified as SL-based heatmap solvers. The framework operates via a fixed forward process and a learned reverse process. The forward process systematically corrupts a ground-truth solution, $\mathbf{x}_0 = \boldsymbol{x}_g^\star$, by injecting noise over T timesteps to produce a purely random vector $\mathbf{x}_T$. The reverse process is trained to iteratively denoise $\mathbf{x}_T$ back to the original solution $\mathbf{x}_0$, effectively functioning as the heatmap generator $\tilde{\pi}_\theta(\cdot|g)$. A detailed formulation is provided in the Appendix A.

3 Empirical Analysis of Objective Mismatch

Comparing the formulations of the SL objective $\mathcal{L}(\theta)$ and the RL objective $\mathcal{R}(\theta)$ reveals a fundamental disconnect. While $\mathcal{R}(\theta)$ explicitly optimizes the post-decoded cost $c_g(f_g(\tilde{\boldsymbol{x}}))$, $\mathcal{L}(\theta)$ *remains blind to* the non-differentiable decoder f_g and the true cost function c_g—what we term **Decoder-Blindness** and **Cost-Blindness**, respectively. As discussed in Section 2.2, despite these blindnesses, $\mathcal{L}(\theta)$ would be a valid surrogate for $\mathcal{R}(\theta)$ under *perfect imitation of optimal labels for all instances*, in principle. Unfortunately, the polynomial-time forward pass of neural networks fundamentally cannot achieve such exact imitation, owing to the NP-hardness of CO (assuming $P \neq NP$). Consequently, for any practical heatmap-based solver, the objective mismatch is inevitable; minimizing $\mathcal{L}(\theta)$ simply does not guarantee minimizing $\mathcal{R}(\theta)$. Yet previous works have not rigorously analyzed the actual impact of this mismatch. This oversight likely stems from a prevailing intuition that $\mathcal{L}(\theta)$ implicitly compensates for these blindness-induced limitations. Specifically, the SL paradigm tacitly relies on the following two hypotheses:

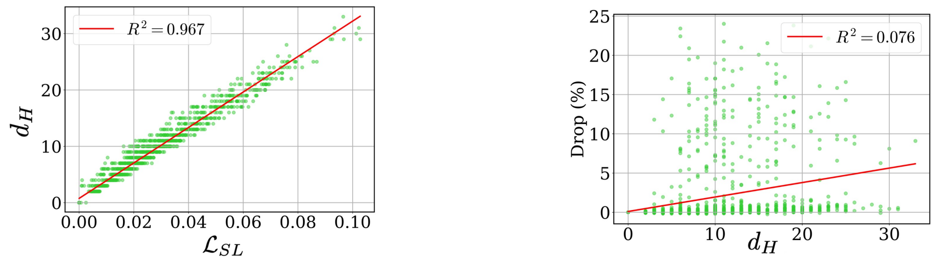

(a) (SL Loss, Hamming distance).

(b) (Hamming distance, Drop).

Figure 1: Scatter plots and correlation analysis for H1 and H2. (a) Surrogate loss $\mathcal{L}_{SL}$ vs. Hamming distance d_{H} (edge disagreements). (b) Hamming distance d_{H} vs. Drop (% cost gap to $\boldsymbol{x}^\star$).

(H1) **Decoder Monotonicity:** A reduction in the SL loss $\mathcal{L}_{SL}$ in (4) leads to a decoded solution $f_g(\tilde{\boldsymbol{x}})$ that is structurally closer to the optimal solution $\boldsymbol{x}^\star$. Here, $d_H(\boldsymbol{x}, \boldsymbol{x}^\star)$ measures the **Hamming distance**, i.e., the number of mispredicted edges. Formally:

$$\mathcal{L}_{SL}(\tilde{\boldsymbol{x}}_A, \boldsymbol{x}^\star) < \mathcal{L}_{SL}(\tilde{\boldsymbol{x}}_B, \boldsymbol{x}^\star) \implies d_H(f_g(\tilde{\boldsymbol{x}}_A), \boldsymbol{x}^\star) < d_H(f_g(\tilde{\boldsymbol{x}}_B), \boldsymbol{x}^\star). \tag{6}$$

(H2) **Cost Smoothness:** A higher structural similarity to the optimal solution $\boldsymbol{x}^\star$ directly translates into a lower solution cost, the ultimate objective of CO. Formally, for any two decoded solutions $\boldsymbol{x}_A$ and $\boldsymbol{x}_B$:

$$d_H(\boldsymbol{x}_A, \boldsymbol{x}^\star) < d_H(\boldsymbol{x}_B, \boldsymbol{x}^\star) \implies c_g(\boldsymbol{x}_A) < c_g(\boldsymbol{x}_B). \tag{7}$$

If both hypotheses held universally, $\mathcal{L}(\theta)$ would be a valid objective for $\mathcal{R}(\theta)$. In Figure 1, we test them empirically using a well-trained SL-based heatmap solver, DIFUSCO (Sun & Yang, 2023). Regarding H1, Figure 1a shows a strong but imperfect correlation—accurate heatmaps do not always yield solutions structurally close to the optimum. More critically, contradicting H2, Figure 1b reveals a near-zero correlation between this structural proximity and the final solution cost. This disconnect reflects the complex landscape of CO, where structural proximity to the optimal solution bears little relation to the solution cost. Collectively, these findings expose the fundamental inadequacy of the imitation-centric SL paradigm for heatmap-based solvers, underscoring the necessity of a training framework that explicitly incorporates both decoder behavior f_g and true cost feedback c_g.

4 Methods

We propose an RL fine-tuning framework that correctly aligns a pre-trained diffusion model $\pi_{\theta_{SL}}$, trained with the SL objective $\mathcal{L}(\theta)$. Our goal is to fine-tune the pre-trained diffusion model $\pi_{\theta_{SL}}$ via RL with the correct objective $\mathcal{R}(\theta)$, yielding $\pi_{\theta_{RL}}$.

4.1 MDP for Correct Training Objective

To address the limitations of the SL objective from Decoder- and Cost-Blindness, we propose a novel MDP formulation that integrates cost c_g and decoder f_g into the fine-tuning process of heatmap-based diffusion solvers. We formulate the denoising process as a Markov Decision Process (MDP), represented by the tuple $(\mathcal{S}, \mathcal{A}, P, \rho_0, R)$. Here, $\mathbf{s} \in \mathcal{S}$ represents a state in the state space $\mathcal{S}$, and $\mathbf{a} \in \mathcal{A}$ denotes an action in the action space $\mathcal{A}$. The state transition distribution is given by $P(\mathbf{s}_{t+1} \mid \mathbf{s}_t, \mathbf{a}_t)$, $\rho_0(\mathbf{s}_0)$ defines the initial state distribution, and $R(\mathbf{s}_t, \mathbf{a}_t)$ represents the reward function. The objective of reinforcement learning is to train the heatmap generator $\tilde{\pi}_\theta$ that maximizes the cumulative sum of rewards.

$$\begin{aligned} \mathbf{s}_t &\triangleq (g, T-t, \mathbf{x}_{T-t}), & \mathbf{a}_t &\triangleq \mathbf{x}_{t-1}, \\ \tilde{\pi}_\theta(\mathbf{a}_t \mid \mathbf{s}_t) &\triangleq p_\theta(\mathbf{x}_{t-1} \mid \mathbf{x}_t, g), & P(\mathbf{s}_{t+1} \mid \mathbf{s}_t, \mathbf{a}_t) &\triangleq (\delta_g, \delta_{T-t-1}, \delta_{\mathbf{x}_{T-t-1}}), \\ \rho_0(\mathbf{s}_T) &\triangleq \left(g, T, \mathrm{Bern}(\boldsymbol{p} = 0.5^{N_g})\right), & R(\mathbf{s}_t, \mathbf{a}_t) &\triangleq \begin{cases} -c_g(f_g(\mathbf{x}_0)) & \text{if } t = T, \\ 0 & \text{otherwise.} \end{cases} \end{aligned} \tag{8}$$

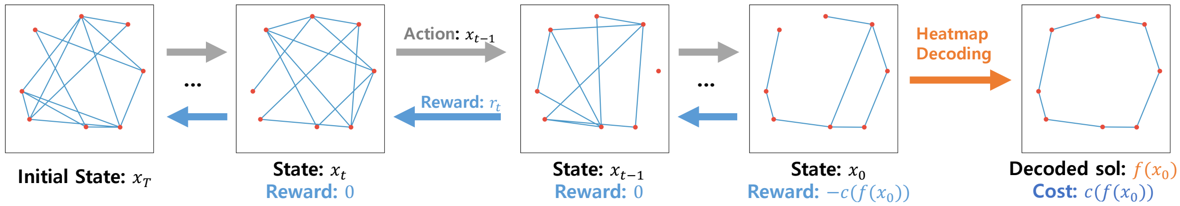

Figure 2: The denoising process formulated as an MDP with initial noise $\mathbf{x}_T \sim \text{Bern}(\boldsymbol{p} = 0.5^N)$.

We define $\text{Bern}(\mathbf{p})$ as a Bernoulli distribution with vector probabilities $\mathbf{p}$ for sampling the initial noise $\mathbf{x}_T$, and δ_y denotes the Dirac delta distribution centered at y. To train the heatmap generator $\tilde{\pi}_\theta$, we apply REINFORCE (Williams, 1992) to optimize the iterative denoising procedure using the learning objective:

$$\nabla_\theta \mathcal{R}(\theta) = \mathbb{E}\left[\sum_{t=1}^{T} \nabla_\theta \log \tilde{\pi}_\theta \left(\mathbf{x}_{t-1} \mid \mathbf{x}_t, g\right) R_t\right] \text{ where } R_t = -c_g\left(f_g(\mathbf{x}_0)\right). \tag{9}$$

By explicitly incorporating both the non-differentiable decoder f_g and the true cost c_g into the reward, our framework directly resolves both **Decoder-Blindness** and **Cost-Blindness**, while benefiting from the training stability provided by the SL initialization. We note that when $T = 1$, this formulation reduces to a single-step MDP, making our framework model-agnostic and applicable to general SL-based heatmap solvers beyond diffusion models (see Appendix D).

4.2 Standard and Label-Centered Reward Strategies

We investigate two distinct reward formulation strategies for CADO: the **Standard Reward (SR)**, which adopts the canonical reward formulation in NCO, and the **Label-Centered Reward (LCR)**, a novel design that strategically exploits the cost information from the pre-training data.

Standard Reward (SR). Our default approach utilizes the negative of the true solution cost directly as the reward signal. To stabilize training and reduce variance, we apply standard batch-wise reward normalization. Crucially, this label-free formulation enables self-sufficient learning through trial-and-error exploration, offering a practical alternative to LCR when labeled solutions are limited while maintaining competitive performance.

Label-Centered Reward (LCR). We propose the Label-Centered Reward (LCR) to further leverage the valuable information embedded in the SL dataset. Rather than direct imitation—which suffers from the objective mismatch discussed earlier—LCR repurposes the *ground-truth solution cost* $b_\mathcal{D}(g)$ *as an instance-specific baseline*. We define the label-centered reward function as the negative optimality gap:

$$R_t = -\left(c_g(f_g(\mathbf{x}_0)) - b_\mathcal{D}(g)\right). \tag{10}$$

Notably, since the baseline $b_\mathcal{D}(g)$ depends solely on the problem instance g and is independent of the policy's actions, it remains a theoretically *unbiased baseline*, ensuring that the policy gradient remains consistent with the true cost minimization objective, regardless of label optimality. This property is practically significant in CO, where acquiring large-scale, optimal training datasets is often computationally prohibitive due to NP-hardness. In this work, we evaluate both variants; for LCR, we strictly reuse the existing SL pre-training dataset to ensure a fair comparison.

4.3 LoRA with Selective Layer Fine-Tuning

To achieve parameter-efficient and stable RL fine-tuning, we employ a hybrid training strategy, **Hybrid Fine-Tuning (Hybrid-FT)**, for our diffusion model architecture comprising an input layer, 12 GNN layers, and an output layer. We apply **Low-Rank Adaptation (LoRA)** (Hu et al., 2022) to the input layer and the first 11 GNN layers, preserving robust pre-trained features by introducing only a small set of trainable low-rank matrices. For layers most critical to final heatmap generation—the final GNN layer and the output layer—we employ **Selective Layer Fine-Tuning (Selective-FT)**, retraining all parameters in these layers. This hybrid approach enhances training stability and memory efficiency without performance degradation.

5 Related Work

Neural Combinatorial Optimization Solvers. Neural approaches to CO generally fall into two categories: autoregressive and heatmap-based solvers. Autoregressive solvers construct solutions sequentially (Kool et al., 2019; Kwon et al., 2020; Kim et al., 2022; Chalumeau et al., 2023; Dernedde et al., 2024; Meng et al., 2025; Liao et al., 2025; Fang et al., 2025; Chalumeau et al., 2025; Verdù et al., 2025), a process amenable to RL but constrained by high inference latency as problem size scales. In contrast, heatmap-based solvers generate a solution in a one-shot manner, enabling highly efficient parallel inference. While early attempts to train these solvers using RL (Qiu et al., 2022) or unsupervised learning (Min et al., 2024; Sanokowski et al., 2024) often yielded limited performance gains for large-scale CO, recent supervised learning (SL) approaches utilizing powerful generative models—such as diffusion models (Graikos et al., 2022; Sun & Yang, 2023; Wang et al., 2025)—have achieved state-of-the-art results. Other lines of work explore divide-and-conquer (Ye et al., 2024; Zheng et al., 2024) and destroy-and-repair (Li et al., 2025) strategies for large-scale problems.

The Objective Mismatch in SL-Based Heatmap Solvers. Despite their success, SL-based heatmap solvers face an intrinsic limitation: they are trained to imitate optimal solutions rather than to minimize solution cost. Recent works have begun to scrutinize this limitation. SoftDIST (Xia et al., 2024) highlighted the mathematical mismatch between SL and RL objectives, providing indirect evidence of suboptimal performance by showing that complex diffusion models often perform comparably to simple rule-based heatmap generators. To mitigate this, T2T (Li et al., 2023) and FastT2T (Li et al., 2024) introduced inference-time cost guidance, steering the denoising process toward lower-cost regions. However, these post-hoc methods do not fully achieve true objective alignment: the non-differentiability of the decoder requires them to guide diffusion with a differentiable surrogate cost function, and their effectiveness remains heavily dependent on the quality of the underlying pre-trained model. Our work differs from prior studies in two critical aspects. First, whereas previous research primarily observed the mathematical discrepancy between objectives, we demonstrate that this mismatch indeed leads to significant performance degradation. Second, we propose a principled resolution to this objective mismatch via CADO, a reinforcement learning fine-tuning framework.

RL Fine-Tuning for Diffusion Models. RL fine-tuning for diffusion models has largely focused on text-to-image generation (Fan et al., 2023; Lee et al., 2023; Wallace et al., 2024), utilizing learned rewards and KL regularization to align with human preferences. We diverge from this paradigm by applying RL fine-tuning to diffusion-based CO solvers. A key advantage of CO over image synthesis is the availability of exact cost functions and deterministic decoders. This allows us to optimize the true CO objective directly, eliminating reliance on potentially unstable learned rewards or KL constraints. Moreover, we propose *Label-Centered Reward* for better utilization of ground-truth data and *Hybrid Fine-Tuning* to enable the efficient adaptation of large-scale GNNs.

6 Experiment

The experiments are conducted using eight NVIDIA L40 GPUs for training and one L40 GPU for testing, along with an AMD EPYC 7413 24-Core Processor.

6.1 Experiment Settings

Problems and Datasets. We evaluate CADO on widely adopted benchmarks for the Traveling Salesman Problem (TSP) and Maximum Independent Set (MIS). For TSP, we utilize standard datasets ranging from 100 to 10k nodes. For MIS, we employ the SATLIB (MIS-SAT) and Erdős-Rényi (MIS-ER) graph benchmarks. All experiments follow standard train/test protocols established in prior works (Kool et al., 2019; Fu et al., 2021; Sun & Yang, 2023).

Evaluation Metrics. We assess our model and other baselines using three metrics. (1) **Cost**: For TSP, we measure the average tour length (lower is better). For MIS, we measure the average size of the independent set (higher is better). (2) **Drop**: We calculate the average drop (optimality gap) between the model-generated solutions and optimal solutions. (3) **Time**: We record the total runtime during testing.

Inference Strategies. To transform heatmaps into feasible solutions, we follow the conventional decoding and post-hoc refinement protocols adopted by prevailing heatmap-based solvers (Qiu et al., 2022; Sun & Yang, 2023; Li et al., 2023; Wang et al., 2025). For MIS, we utilize a greedy decoder without further refinement. For TSP, we utilize a greedy decoder and optionally apply post-hoc refinement using the 2-opt heuristic (Lin & Kernighan, 1973) or Monte Carlo Tree Search (MCTS). Furthermore, we incorporate the Local Rewrite (LR) strategy to iteratively enhance solution quality via partial noise injection and reconstruction. Crucially, unlike T2T (Li et al., 2023) which relies on gradient-based cost-guided search (CS) during rewriting, our method operates without such auxiliary guidance, relying solely on the robust heatmap learned via RL fine-tuning. We also evaluate **CADO-L**, an ablated version of CADO that excludes LR. This variant enables a direct evaluation of our RL fine-tuning, isolating the effect of additional search techniques, while *reducing computational overhead to 40%* of baseline methods. All CADO results are the average of 4 independent runs.

Baselines. We compare our method with the following methods: (1) **Exact Solvers**: Concorde (Applegate et al., 2006) and Gurobi (Gurobi Optimization, LLC, 2020); (2) **Heuristics**: LKH3 (Applegate et al., 2006), KaMIS (Lamm et al., 2016), Farthest Insertion; (3) **Supervised learning (SL):** GCN (Joshi et al., 2019), BQ (Drakulic et al., 2023), LEHD (Luo et al., 2023), DIFUSCO (Sun & Yang, 2023), T2T (Li et al., 2023), DEITSP (Wang et al., 2025), FastT2T (Li et al., 2024), DRHG (Li et al., 2025); (4) **Reinforcement learning (RL)**: AM (Kool et al., 2019), POMO (Hottung et al., 2022), DIMES (Qiu et al., 2022), COMPASS (Chalumeau et al., 2023), ICAM (Zhou et al., 2024), GLOP (Ye et al., 2024), UDC (Zheng et al., 2024), HierTSP (Goh et al., 2024), LRBS (Verdù et al., 2025), MEMENTO (Chalumeau et al., 2025); (5) **Unsupervised learning (UL)** : GFlowNets (Zhang et al., 2023), UTSP (Min et al., 2024).

6.2 Addressing the Objective Mismatch in SL via RL

As discussed in Section 3 (see Figure 1), the two blindnesses in the SL objective cause objective mismatch, which can degrade performance. In this section, we empirically evaluate whether our proposed framework can effectively address these blindnesses.

Cost-Blindness. Figure 3 provides compelling evidence that the SL objective is a flawed proxy for the true CO objective. It showcases a striking divergence during RL fine-tuning: while CADO-L slashes the drop by a remarkable 58.5% (from 0.6% to 0.25%), the SL loss simultaneously *increases*. This inverse relationship decisively validates our central claim: *merely imitating optimal solutions is an ineffective and potentially counterproductive strategy for CO*. Furthermore, this result demonstrates that CADO's performance gain is not a byproduct of an additional training process, but a direct consequence of correct alignment with the true, post-decoding solution cost.

Decoder-Blindness. We next validate that CADO's decoder-aware objective indeed overcomes **Decoder-Blindness** in SL (Figure 1a). To demonstrate this, we test the standard SL-trained DIFUSCO with two

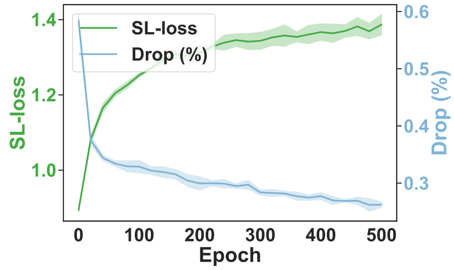

Figure 3: Learning curve of CADO-L for MIS-SAT. The average of 4 independent runs.

Algorithm	Test (`Grdy`) Drop ↓	Test (`NN`) Drop ↓
DIFUSCO	1.62%	2.32%
CADO-L (`Grdy`)	**0.19%**	0.34%
CADO-L (`NN`)	0.31%	**0.31%**

Table 1: Impact of decoder-aware training.

Algorithm	Type	TSP-100			TSP-500			TSP-1k			TSP-10k		
		Length ↓	Drop ↓	Time	Length ↓	Drop ↓	Time	Length ↓	Drop ↓	Time	Length ↓	Drop ↓	Time
Concorde	Exact	7.76*	-	40m	16.55*	-	38m	23.12*	-	6.7h	-	-	-
LKH-3	Heuristics	7.76	0.00%	1.4h	16.55	0.00%	46m	23.12	0.00%	2.6h	71.77*	-	8.8h
FI	Heuristics	8.72	12.36%	0s	18.30	10.57%	0s	25.72	11.25%	0s	80.59	12.29%	6s
AM	RL+BS	7.95	4.53%	6s	20.02	20.99%	1.5m	31.15	34.8%	3.2m	141.68	97.4%	6.0m
EAN	RL+2-opt	-	-	-	23.75	43.6%	58m	47.73	106%	5.4h	-	-	-
POMO	RL	7.84	1.07%	2s	19.24	16.25%	13h	-	-	-	-	-	-
BQ†	SL	7.79	0.35%	-	16.72	1.18%	0.8m	23.65	2.27%	1.9m	-	-	-
LEHD	SL+RRC20	7.76	0.04%	0.4m	16.66	0.66%	1.6m	23.51	1.70%	11m	-	-	-
ICAM†	RL+Aug8	7.77	0.15%	37s	16.55	0.77%	38s	23.49	1.58%	3.8m	-	-	-
SIL	RL+PRC50	-	-	-	-	-	-	23.46	1.50%	9.0m	73.77	2.78%	10m
DRHG	SL+DR150	**7.76**	**0.00%**	9.0m	16.65	0.62%	2.9m	23.55	1.85%	3.1m	-	-	-
LRBS†	RL	7.76	0.01%	22h	17.19	3.97%	2.0h	25.90	11.89%	8.1h	-	-	-
COMPASS†	RL	-	-	-	16.81	1.60%	-	-	-	-	-	-	-
MEMENTO†	RL	-	-	-	16.80	1.59%	-	-	-	-	-	-	-
GLOP	RL+DC	-	-	-	16.91	1.99%	1.5m	23.84	3.11%	3.0m	75.29	4.90%	1.8m
UDC†	RL+DC	-	-	-	16.78	1.58%	4.0m	23.53	1.78%	8.0m	-	-	-
GCN	SL	8.41	8.38%	6m	29.72	79.6%	6.7m	48.62	110%	29m	-	-	-
UTSP†	UL+MCTS	**7.76**	**0.00%**	1.1m	17.11	3.41%	3.0m	24.14	4.40%	6.7m	-	-	-
SoftDIST	MCTS	-	-	-	16.78	1.44%	1.7m	23.63	2.20%	3.3m	74.03	3.13%	17m
DIMES	RL+MCTS	-	-	-	16.87	1.93%	2.9m	23.73	2.64%	6.9m	74.63	3.98%	30m
DEITSP†‡	SL+2-opt	7.77	0.10%	4.0m	16.90	2.15%	9.3m	23.97	3.68%	42m	-	-	-
FastT2T	SL+CS+2-opt	7.76	0.01%	1.6m	16.66	0.65%	46s	23.35	0.99%	3.5m	-	-	-
DIFUSCO	SL+2-opt	7.78	0.41%	-	16.81	1.55%	5.8m	23.55	1.86%	18m	73.99	3.10%	35m
T2T	SL+CS+2-opt	7.76	0.06%	-	16.68	0.83%	4.8m	23.41	1.26%	18m	-	-	-
CADO	SL+RL+2-opt	7.76	0.06%	5.4m	**16.65**	**0.61%**	1.7m	**23.32**	**0.88%**	3.6m	**73.69**	**2.68%**	13m

Table 2: Results on TSP-100/500/1k/10k. BS: Beam Search, RRC: Random Re-Construct, CS: Cost-guided Search, DC: Divide-and-Conquer. * represents the baseline for computing the drop. The results of models marked with † are evaluated on different test datasets and are taken from their respective papers. ‡ denotes generalization results from models trained on a different distribution.

decoders: a Greedy (`Grdy`) decoder and a simpler Nearest Neighbor (`NN`) decoder. As shown in Table 1, DIFUSCO's performance degrades significantly when switching to the simpler `NN` decoder (1.62% to 2.32%) even though the underlying heatmap remains identical. This implies that the heatmap generation process should be explicitly conditioned on the specific decoder used. In contrast, we train two CADO-L variants, each fine-tuned for one of the decoders. Unlike the static heatmap of DIFUSCO, performance is maximized when the inference decoder aligns with the training objective, confirming CADO-L's ability to learn decoder-specific structural priors. This provides definitive proof that CADO-L's integration of decoder feedback generates heatmaps structured for its paired decoder, directly resolving the flaws from Decoder-Blindness of SL.

6.3 Main Results for Varied CO Benchmarks

We evaluate CADO on widely-used benchmarks for the TSP and the MIS. Across all settings, CADO demonstrates remarkably consistent and superior performance. Notably, this robustness is achieved without extensive, task-specific hyperparameter tuning; we employ a nearly identical configuration for all experiments, adjusting only the number of training epochs. Detailed experimental settings are provided in the Appendix C.

TSP-100/500/1k/10k. Table 2 summarizes the results on TSP instances ranging from 100 to 10k nodes. For a fair comparison, we standardized the computational budget for inference: autoregressive baselines were adjusted to match CADO's inference time, and 2-opt for heatmap-based solvers was capped at 1,000 iterations. Across all scales, CADO consistently outperforms the majority of baselines. Notably on TSP-1k, while the SL-trained DIFUSCO (1.86%) shows marginal improvement over the non-learned SoftDIST (2.20%), CADO achieves a significantly reduced drop of 0.88%, effectively halving the drop of DIFUSCO. On TSP-10k, despite being a one-shot heatmap generator, CADO surpasses divide-and-conquer methods (e.g., GLOP, UDC) explicitly designed for large-scale efficiency.

MIS-SAT/ER. Our approach demonstrates robust superiority on MIS problems, significantly outperforming state-of-the-art baselines across two distinct graph distributions: MIS-SAT and MIS-ER. These widely adopted

Algorithm	Type	SATLIB			ER-[700-800]		
		Size ↑	**Drop ↓**	**Time**	**Size ↑**	**Drop ↓**	**Time**
KaMIS	Heuristics	425.96*	-	38m	44.87*	-	52m
Gurobi	Exact	425.95	0.00%	26m	41.28	-	50m
LwD	RL+S	422.22	0.88%	19m	41.17	8.25%	6.3m
GFlowNets	UL+S	423.54	0.57%	23m	41.14	8.53%	2.9m
UDC	RL+DC	-	-	-	42.88	4.44%	21m
Intel	SL	420.66	1.48%	23m	34.86	22.31%	6.1m
DIMES	RL	421.24	1.11%	24m	38.24	14.78%	6.1m
DIFUSCO	SL	424.56	0.33%	8.3m	36.55	18.53%	8.8m
T2T	SL+CS	425.02	0.22%	8.1m	39.56	11.83%	8.5m
FastT2T	SL+CS	-	-	-	40.60	9.52%	41s
CADO	SL+RL	**425.43**	**0.12%**	6.5m	**43.62**	**2.78%**	1.8m

Table 3: Results on SATLIB and ER-[700-800].

benchmarks inherently present disparate pre-training qualities: the SL baseline achieves high accuracy on MIS-SAT (0.33% drop) but fails significantly on MIS-ER (18.53% drop).

Despite this drastic disparity in initial model quality, CADO demonstrates universal robustness. While it refines the already strong MIS-SAT model, its impact is most profound in the challenging MIS-ER regime. Here, CADO achieves a drop of only 2.78%, representing an 85% gap reduction from the pretrained DIFUSCO (18.53%) and a 70% improvement over the previous best method, FastT2T (9.52%). This substantial margin underscores the effectiveness of correcting the objective mismatch, and empirically corroborates our analysis in Section 3: the objective mismatch manifests most severely when heatmap-based SL solvers yield highly suboptimal heatmaps, an issue that CADO dramatically mitigates through its correct objective alignment.

6.4 Detailed Analysis of Heatmap-Based Solvers

This section dissects the core methodologies of heatmap-based solvers, distinguishing between SL, RL, post-hoc cost guidance, and our proposed RL fine-tuning. To rigorously isolate the intrinsic efficacy of each learning objective, we introduce two control baselines: (1) **RL-Scratch**, trained from scratch to evaluate the necessity of SL initialization, and (2) **DIFUSCO+SFT**, which extends SL training by 50% additional epochs to ensure that CADO's improvements are not merely due to extended training. We disable all auxiliary search heuristics (e.g., 2-opt, MCTS) to ensure a controlled comparison of the underlying heatmap-based solvers.

Pure RL approaches, DIMES and RL-Scratch, exhibit significantly inferior performance compared to SL-based counterparts. This result underscores that SL pre-training serves as a requisite warm-start for navigating the high-dimensional combinatorial landscape. On the other hand, the SL-based DIFUSCO+SFT yields negligible improvements over DIFUSCO and remains significantly inferior to cost-integrated baselines. This

Algorithm	Type	TSP-500 Drop ↓	TSP-1k Drop ↓	MIS-SAT Drop ↓	MIS-ER Drop ↓
DIMES	RL	15.0%	15.0%	1.1%	14.8%
RL-Scratch	RL	18.0%	17.5%	0.88%	26.4%
DIFUSCO	SL	11.2%	11.2%	0.33%	18.5%
DIFUSCO+SFT	SL	10.1%	12.3%	0.29%	12.4%
T2T	SL+CS+LR	6.9%	9.8%	0.22%	11.8%
FastT2T (5,3)	SL+CS+LR	5.5%	8.9%	-	9.5%
CADO-L	SL+RL	**3.0%**	**6.1%**	**0.16%**	**4.3%**
CADO	SL+RL+LR	**1.3%**	**4.0%**	**0.12%**	**2.8%**

Table 4: Comparisons between different cost information integration strategies for Heatmap-Based Solvers. SL/RL stands for Supervised Learning and Reinforcement Learning, respectively. CS stands for cost-guided search. LR stands for Local Rewrite.

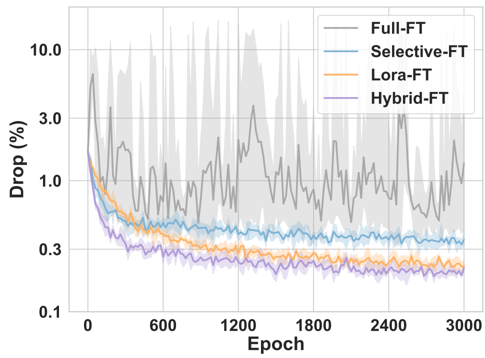

Figure 4: Learning curve of various fine-tuning methods. The result is the average of 4 independent runs.

Algorithm	TSP-100 Drop ↓	TSP-500 Drop ↓	MIS-SAT Drop ↓
DIFUSCO	1.01%	11.2%	0.33%
DIFUSCO+SFT	1.05%	10.1%	0.29%
CADO-L (w/ SR)	**0.22%**	**3.3%**	**0.19%**
CADO-L (w/ LCR)	**0.19%**	**3.0%**	**0.16%**
Improvement of LCR (%)	15.8%	10.0%	18.8%

Table 5: Ablation Study for Label-Centered Reward.

performance plateau implies that the sub-optimality of SL solvers is not merely a symptom of insufficient training steps, but a consequence of the fundamental objective mismatch inherent in the SL objective itself.

In comparing cost integration strategies, CADO-L outperforms T2T and FastT2T even in its standalone form without Local Rewrite (LR), while these baselines require LR despite its additional computational overhead. When LR is applied to CADO as well, the performance gap widens further. This leads to a clear conclusion: fundamentally realigning the generative prior via RL fine-tuning is far more effective than applying post-hoc guidance via surrogate cost functions. We provide a more comprehensive comparison with other cost-aware heatmap-based solvers in Appendix D.

We also validate CADO's framework on other SL-based heatmap solvers in Appendix D. Crucially, CADO operates as a model-agnostic framework capable of enhancing various heatmap-based SL solvers beyond diffusion models. For instance, applying CADO to the pre-trained FastT2T (1,0), a general heatmap solver that operates via a single forward pass rather than a diffusion process, yields substantial performance gains, as detailed in Tables 13 and 14. This demonstrates that our framework is a versatile tool that effectively resolves the objective mismatch for a wide range of heatmap-based solvers.

6.5 Ablation Study

Impact of Reward Strategies. We compare CADO with SR and LCR in Table 5. The results reveal two key insights. First, both variants substantially outperform the original DIFUSCO and extended supervised fine-tuning (DIFUSCO+SFT). Notably, even the label-free CADO (w/ SR) alone strongly outperforms all baselines, confirming that RL-based objective alignment is the primary driver of performance. Second, CADO (w/ LCR) yields an additional 10.0%–18.8% improvement over CADO (w/ SR). This demonstrates that leveraging ground-truth labels as an unbiased baseline effectively achieves correct objective alignment rather than flawed imitation.

Analysis of LoRA and Selective Layer Fine-Tuning. We compare several parameter-efficient fine-tuning strategies on the TSP-100. As illustrated in Figure 4, naively fine-tuning all parameters (Full-FT) proves highly unstable. Applying only LoRA (LoRA-FT) ensures stability but suffers from slow initial convergence. Conversely, fine-tuning only the final, selective layers (Selective-FT) yields rapid initial gains but quickly plateaus due to limited expressive power to adapt the entire model. Our Hybrid-FT strategy, which judiciously combines LoRA for backbone layers and full fine-tuning for final layers, resolves these trade-offs. It achieves consistently superior results, demonstrating both fast initial convergence and the best final performance. These results validate Hybrid-FT as a practical RL fine-tuning approach that maintains both stability and strong expressive power for large-scale GNNs.

Algorithm	TSPLIB (50–200)	
	Drop ↓	**Time**
Concorde	0.00%	-
AM	3.93%	13.2s
POMO	1.39%	2.9s
Sym-NCO	1.92%	3.0s
ELG	1.14%	6.7s
HierTSP	1.78%	3.9s
DIFUSCO	1.28%	20.6s
T2T	0.90%	29.0s
DEITSP	0.78%	8.5s
CADO	**0.46%**	22.1s

Table 6: Generalization results on TSPLIB (50–200).

Algorithm	Drop ↓
DIFUSCO	11.84%
T2T	6.99%
CADO (w/ SR)	**1.86%**
CADO (w/ LCR)	**1.71%**

Table 7: Robustness under low-quality training on TSP-100 without the 2-opt heuristic.

6.6 Analysis on Robustness and Generalization

6.6.1 Generalization to Real-World Dataset

To evaluate the generalization ability of CADO to unseen real-world scenarios, we test the TSP-100-trained model on **TSPLIB (50–200 nodes)**, a widely used real-world TSP benchmark. As shown in Table 6, CADO outperforms other baselines with a 0.46% drop, reducing the gap by approximately 41% compared to the previous best. To further validate CADO in a larger-scale setting, we also test the TSP-500-trained model on **TSPLIB (200–1000 nodes)**, where CADO again achieves the highest score among diffusion-based solvers. Detailed results for all TSPLIB benchmarks are provided in Table 16 in Appendix E.

6.6.2 Performance Under Low-Quality Training Data

We evaluate the robustness of heatmap-based solvers using a suboptimal TSP-100 dataset generated by a time-limited LKH solver, which exhibits a known 1.36% drop. This setting mirrors practical scenarios where obtaining optimal solutions for large-scale CO problems is computationally intractable, necessitating the use of suboptimal solutions. As shown in Table 7, imitation-centric methods suffer severely from data quality degradation. DIFUSCO exhibits error amplification, deteriorating to an 11.84% gap, while even T2T's post-hoc guidance fails to fully mitigate the flawed pre-training (6.99%).

In contrast, CADO demonstrates exceptional robustness. CADO (w/ SR) achieves a drop of only 1.86%, significantly outperforming all other baselines. Notably, leveraging suboptimal labels via the Label-Centered Reward further boosts performance to 1.71%. This outcome is particularly surprising, as it demonstrates that the Label-Centered Reward remains superior to the Standard Reward even when the labels are noisy. This empirically aligns with our theoretical claim in Section 4.2 that the Label-Centered Reward can serve as an unbiased baseline even with suboptimal labels, confirming its practical utility in real-world scenarios.

7 Conclusion

In this work, we present the first direct evidence that objective mismatch—manifested as Decoder- and Cost-Blindness—acts as a fundamental bottleneck in supervised learning for heatmap-based CO solvers. To address this, we propose CADO (**C**ost-**A**ware **D**iffusion models for **O**ptimization), a reinforcement learning fine-tuning framework that explicitly realigns the diffusion process with the true CO objective. We introduce Label-Centered Reward, a novel reward formulation for CO that repurposes pre-training labels to ensure precise objective alignment rather than mere imitation. Additionally, our Hybrid Fine-Tuning strategy facilitates the stable and efficient adaptation of large-scale GNN architectures. Extensive experiments demonstrate that CADO achieves a new state-of-the-art across TSP and MIS benchmarks while exhibiting exceptional robustness to suboptimal datasets. Ultimately, this work signifies a pivotal shift in heatmap-based CO solvers: moving beyond rigid structural imitation toward direct, cost-aware optimization.

References

David Applegate, Robert Bixby, Vasek Chvatal, and William Cook. Concorde TSP solver. `http://www.math.uwaterloo.ca/tsp/concorde.html`, 2006.

Jacob Austin, Daniel D. Johnson, Jonathan Ho, Daniel Tarlow, and Rianne van den Berg. Structured denoising diffusion models in discrete state-spaces. In *Advances in Neural Information Processing Systems*, volume 34, pp. 17981–17993, 2021.

Xavier Bresson and Thomas Laurent. An experimental study of neural networks for variable graphs. In *International Conference on Learning Representations, Workshop Track*, 2018.

Felix Chalumeau, Shikha Surana, Clément Bonnet, Nathan Grinsztajn, Arnu Pretorius, Alexandre Laterre, and Tom Barrett. Combinatorial optimization with policy adaptation using latent space search. In *Advances in Neural Information Processing Systems*, volume 36, pp. 7947–7959, 2023.

Felix Chalumeau, Refiloe Shabe, Noah De Nicola, Arnu Pretorius, Thomas D. Barrett, and Nathan Grinsztajn. Memory-enhanced neural solvers for routing problems. In *Advances in Neural Information Processing Systems*, volume 38, 2025.

Paulo R. de O. da Costa, Jason Rhuggenaath, Yingqian Zhang, and Alp Akcay. Learning 2-opt heuristics for the traveling salesman problem via deep reinforcement learning. In *Asian Conference on Machine Learning*, volume 129 of *Proceedings of Machine Learning Research*, pp. 465–480, 2020.

Tim Dernedde, Daniela Thyssens, Sören Dittrich, Maximilian Stubbemann, and Lars Schmidt-Thieme. MoCO: A learnable meta optimizer for combinatorial optimization. *arXiv preprint arXiv:2402.04915*, 2024.

Darko Drakulic, Sofia Michel, Florian Mai, Arnaud Sors, and Jean-Marc Andreoli. BQ-NCO: Bisimulation quotienting for efficient neural combinatorial optimization. In *Advances in Neural Information Processing Systems*, volume 36, 2023.

Ying Fan, Olivia Watkins, Yuqing Du, Hao Liu, Moonkyung Ryu, Craig Boutilier, Pieter Abbeel, Mohammad Ghavamzadeh, Kangwook Lee, and Kimin Lee. DPOK: Reinforcement learning for fine-tuning text-to-image diffusion models. In *Advances in Neural Information Processing Systems*, volume 36, pp. 79858–79885, 2023.

Zhanhong Fang, Debing Wang, Jinbiao Chen, Jiahai Wang, and Zizhen Zhang. UCPO: A universal constrained combinatorial optimization method via preference optimization. *arXiv preprint arXiv:2511.10148*, 2025.

Zhang-Hua Fu, Kai-Bin Qiu, and Hongyuan Zha. Generalize a small pre-trained model to arbitrarily large TSP instances. In *AAAI Conference on Artificial Intelligence*, pp. 7474–7482, 2021.

Simon Geisler, Johanna Sommer, Jan Schuchardt, Aleksandar Bojchevski, and Stephan Günnemann. Generalization of neural combinatorial solvers through the lens of adversarial robustness. In *International Conference on Learning Representations*, 2022.

Yong Liang Goh, Zhiguang Cao, Yining Ma, Yanfei Dong, Mohammed Haroon Dupty, and Wee Sun Lee. Hierarchical neural constructive solver for real-world TSP scenarios. In *ACM SIGKDD Conference on Knowledge Discovery and Data Mining*, pp. 884–895, 2024.

Alexandros Graikos, Nikolay Malkin, Nebojsa Jojic, and Dimitris Samaras. Diffusion models as plug-and-play priors. In *Advances in Neural Information Processing Systems*, volume 35, pp. 14715–14728, 2022.

Gurobi Optimization, LLC. Gurobi optimizer reference manual. `http://www.gurobi.com`, 2020.

Keld Helsgaun. An extension of the Lin-Kernighan-Helsgaun TSP solver for constrained traveling salesman and vehicle routing problems. *Roskilde University*, pp. 24–50, 2017.

André Hottung, Yeong-Dae Kwon, and Kevin Tierney. Efficient active search for combinatorial optimization problems. In *International Conference on Learning Representations*, 2022.

Edward J. Hu, Yelong Shen, Phillip Wallis, Zeyuan Allen-Zhu, Yuanzhi Li, Shean Wang, Lu Wang, and Weizhu Chen. LoRA: Low-rank adaptation of large language models. In *International Conference on Learning Representations*, 2022.

Sergey Ioffe and Christian Szegedy. Batch normalization: Accelerating deep network training by reducing internal covariate shift. In *International Conference on Machine Learning*, volume 37, pp. 448–456, 2015.

Chaitanya K. Joshi, Thomas Laurent, and Xavier Bresson. An efficient graph convolutional network technique for the travelling salesman problem. *arXiv preprint arXiv:1906.01227*, 2019.

Richard M. Karp. On the computational complexity of combinatorial problems. *Networks*, 5(1):45–68, 1975.

Minsu Kim, Junyoung Park, and Jinkyoo Park. Sym-NCO: Leveraging symmetricity for neural combinatorial optimization. In *Advances in Neural Information Processing Systems*, volume 35, 2022.

Wouter Kool, Herke van Hoof, and Max Welling. Attention, learn to solve routing problems! In *International Conference on Learning Representations*, 2019.

Alex Krizhevsky and Geoffrey Hinton. Convolutional deep belief networks on CIFAR-10. *Unpublished manuscript*, 40(7):1–9, 2010.

Yeong-Dae Kwon, Jinho Choo, Byoungjip Kim, Iljoo Yoon, Seungjai Min, and Youngjune Gwon. POMO: Policy optimization with multiple optima for reinforcement learning. In *Advances in Neural Information Processing Systems*, volume 33, 2020.

Sebastian Lamm, Peter Sanders, Christian Schulz, Darren Strash, and Renato F. Werneck. Finding near-optimal independent sets at scale. In *Workshop on Algorithm Engineering and Experiments*, pp. 138–150, 2016.

Kimin Lee, Hao Liu, Moonkyung Ryu, Olivia Watkins, Yuqing Du, Craig Boutilier, Pieter Abbeel, Mohammad Ghavamzadeh, and Shixiang Shane Gu. Aligning text-to-image models using human feedback. *arXiv preprint arXiv:2302.12192*, 2023.

Ke Li, Fei Liu, Zhenkun Wang, and Qingfu Zhang. Destroy and repair using hyper-graphs for routing. In *AAAI Conference on Artificial Intelligence*, volume 39, pp. 18341–18349, 2025.

Yang Li, Jinpei Guo, Runzhong Wang, and Junchi Yan. From distribution learning in training to gradient search in testing for combinatorial optimization. In *Advances in Neural Information Processing Systems*, volume 36, 2023.

Yang Li, Jinpei Guo, Runzhong Wang, Hongyuan Zha, and Junchi Yan. Fast T2T: Optimization consistency speeds up diffusion-based training-to-testing solving for combinatorial optimization. In *Advances in Neural Information Processing Systems*, volume 37, pp. 30179–30206, 2024.

Zijun Liao, Jinbiao Chen, Debing Wang, Zizhen Zhang, and Jiahai Wang. BOPO: Neural combinatorial optimization via best-anchored and objective-guided preference optimization. *arXiv preprint arXiv:2503.07580*, 2025.

Shen Lin and Brian W. Kernighan. An effective heuristic algorithm for the traveling-salesman problem. *Operations Research*, 21(2):498–516, 1973.

Fu Luo, Xi Lin, Fei Liu, Qingfu Zhang, and Zhenkun Wang. Neural combinatorial optimization with heavy decoder: Toward large scale generalization. In *Advances in Neural Information Processing Systems*, volume 36, 2023.

Dian Meng, Zhiguang Cao, Yaoxin Wu, Yaqing Hou, Hongwei Ge, and Qiang Zhang. EFormer: An effective edge-based transformer for vehicle routing problems. *arXiv preprint arXiv:2506.16428*, 2025.

Yimeng Min, Yiwei Bai, and Carla P. Gomes. Unsupervised learning for solving the travelling salesman problem. In *Advances in Neural Information Processing Systems*, volume 36, 2024.

Ruizhong Qiu, Zhiqing Sun, and Yiming Yang. DIMES: A differentiable meta solver for combinatorial optimization problems. In *Advances in Neural Information Processing Systems*, volume 35, pp. 25531–25546, 2022.

Sebastian Sanokowski, Sepp Hochreiter, and Sebastian Lehner. A diffusion model framework for unsupervised neural combinatorial optimization. In *International Conference on Machine Learning*, 2024.

Zhiqing Sun and Yiming Yang. DIFUSCO: Graph-based diffusion solvers for combinatorial optimization. In *Advances in Neural Information Processing Systems*, volume 36, pp. 3706–3731, 2023.

Ashish Vaswani, Noam Shazeer, Niki Parmar, Jakob Uszkoreit, Llion Jones, Aidan N. Gomez, Łukasz Kaiser, and Illia Polosukhin. Attention is all you need. In *Advances in Neural Information Processing Systems*, volume 30, 2017.

Federico Julian Camerota Verdù, Lorenzo Castelli, and Luca Bortolussi. Scaling combinatorial optimization neural improvement heuristics with online search and adaptation. In *AAAI Conference on Artificial Intelligence*, volume 39, pp. 27135–27143, 2025.

Juan Pablo Vielma. Mixed integer linear programming formulation techniques. *SIAM Review*, 57(1):3–57, 2015.

Bram Wallace, Meihua Dang, Rafael Rafailov, Linqi Zhou, Aaron Lou, Senthil Purber, Stefano Ermon, Caiming Xiong, Shafiq Joty, and Nikhil Naik. Diffusion model alignment using direct preference optimization. *arXiv preprint arXiv:2311.12908*, 2024.

Mingzhao Wang, You Zhou, Zhiguang Cao, Yubin Xiao, Xuan Wu, Wei Pang, Yuan Jiang, Hui Yang, Peng Zhao, and Yuanshu Li. An efficient diffusion-based non-autoregressive solver for traveling salesman problem. In *ACM SIGKDD Conference on Knowledge Discovery and Data Mining*, 2025.

Ronald J Williams. Simple statistical gradient-following algorithms for connectionist reinforcement learning. *Machine Learning*, 8(3–4):229–256, 1992.

Yaoxin Wu, Wen Song, Zhiguang Cao, Jie Zhang, and Andrew Lim. Learning improvement heuristics for solving routing problems. *IEEE Transactions on Neural Networks and Learning Systems*, 33:5057–5069, 2022.

Yifan Xia, Xianliang Yang, Zichuan Liu, Zhihao Liu, Lei Song, and Jiang Bian. Position: Rethinking post-hoc search-based neural approaches for solving large-scale traveling salesman problems. In *International Conference on Machine Learning*, 2024.

Keyulu Xu, Weihua Hu, Jure Leskovec, and Stefanie Jegelka. How powerful are graph neural networks? In *International Conference on Learning Representations*, 2019.

Haoran Ye, Jiarui Wang, Helan Liang, Zhiguang Cao, Yong Li, and Fanzhang Li. GLOP: Learning global partition and local construction for solving large-scale routing problems in real-time. In *AAAI Conference on Artificial Intelligence*, 2024.

Dinghuai Zhang, Hanjun Dai, Nikolay Malkin, Aaron C. Courville, Yoshua Bengio, and Ling Pan. Let the flows tell: Solving graph combinatorial optimization problems with GFlowNets. In *Advances in Neural Information Processing Systems*, volume 36, pp. 11952–11969, 2023.

Zhi Zheng, Changliang Zhou, Xialiang Tong, Mingxuan Yuan, and Zhenkun Wang. UDC: A unified neural divide-and-conquer framework for large-scale combinatorial optimization problems. In *Advances in Neural Information Processing Systems*, volume 37, 2024.

Changliang Zhou, Xi Lin, Zhenkun Wang, Xialiang Tong, Mingxuan Yuan, and Qingfu Zhang. Instance-conditioned adaptation for large-scale generalization of neural combinatorial optimization. *arXiv preprint arXiv:2405.01906*, 2024.

A Training objective in Diffusion Model

In this section, we describe the supervised learning approach for training a diffusion-based heatmap solver $\tilde{\pi}_\theta(\boldsymbol{x}|g)$, following the methodology established by Sun & Yang (2023). The diffusion process consists of a forward noising procedure and a reverse denoising procedure. During the forward process, noise is gradually added to the initial solution until it is fully transformed into random noise, creating a sequence of latent variables $\mathbf{x_0}, \mathbf{x_1}, \ldots, \mathbf{x_T}$ where $\mathbf{x}_0 = \boldsymbol{x}_g^\star$ in CO and $\mathbf{x}_T$ is completely random noise. The forward noising process is defined by $q(\mathbf{x_{1:T}}|\mathbf{x_0}) = \prod_{t=1}^{T} q(\mathbf{x_t}|\mathbf{x_{t-1}})$. Then, during the reverse denoising procedure, a model is trained to denoise this random noise $\mathbf{x_T}$ back to the high-quality solution $\mathbf{x}_0$. The reverse process is modeled as $\tilde{\pi}_\theta(\mathbf{x_{0:T}}|g) = \tilde{p}(\mathbf{x_T}) \prod_{t=1}^{T} \tilde{\pi}_\theta(\mathbf{x_{t-1}}|\mathbf{x_t}, g)$, with θ representing the model parameters, and this reverse model is later used as a heatmap-based solver.

The training objective is to match $p_\theta(\mathbf{x_0}|g)$ with the high-quality data distribution $q(\mathbf{x_0}|g)$, by minimizing the variational upper bound of the negative log-likelihood:

$$\mathcal{L}(\theta) = \mathbb{E}_q\Big[-\log \tilde{\pi}_\theta(\mathbf{x_0}|\mathbf{x_1}, g) + \sum_{t=2}^{T} D_{KL}(q(\mathbf{x_{t-1}}|\mathbf{x_t}, \mathbf{x_0}) \| \tilde{\pi}_\theta(\mathbf{x_{t-1}}|\mathbf{x_t}, g))\Big]. \tag{11}$$

In CO, considering that each entry of the optimization variable $\boldsymbol{x}$ is an indicator of whether to select a node or an edge, each entry can also be represented as a one-hot $\{0,1\}^2$ when modeled with a Bernoulli distribution. Therefore, for diffusion process, $\boldsymbol{x}$ turns into N one-hot vectors $\mathbf{x_0} \in \{0,1\}^{N\times 2}$. Then, a discrete diffusion model (Austin et al., 2021) is utilized. Specifically, at each time step t, the process transitions from $\mathbf{x_{t-1}}$ to $\mathbf{x_t}$ defined by:

$$q(\mathbf{x_t}|\mathbf{x_{t-1}}) = \mathrm{Cat}(\mathbf{x_t}; \mathbf{p} = \boldsymbol{x}_{t-1}\mathbf{Q_t}) \tag{12}$$

where the $\mathrm{Cat}(\boldsymbol{x}; \mathbf{p})$ is a categorical distribution over $x \in \{0,1\}^{N\times 2}$ with vector probabilities $\mathbf{p}$ and transition probability matrix $\mathbf{Q_t}$ is:

$$\mathbf{Q_t} = \begin{bmatrix} (1-\beta_t) & \beta_t \\ \beta_t & (1-\beta_t) \end{bmatrix}. \tag{13}$$

Here, β_t represents the noise level at time t. The t-step marginal distribution can be expressed as:

$$q(\mathbf{x_t}|\mathbf{x_0}) = \mathrm{Cat}(\mathbf{x_t}; \mathbf{p} = \mathbf{x_0}\overline{\mathbf{Q}}_\mathbf{t}) \tag{14}$$

where $\overline{\mathbf{Q}}_\mathbf{t} = \mathbf{Q_1}\mathbf{Q_2}, \ldots, \mathbf{Q}_t$. To obtain the distribution $q(\mathbf{x_{t-1}}|\mathbf{x_t}, \mathbf{x_0})$ for the reverse process, Bayes' theorem is applied, resulting in:

$$q(\mathbf{x_{t-1}}|\mathbf{x_t}, \mathbf{x_0}) = \mathrm{Cat}\left(\mathbf{x_{t-1}}; \mathbf{p} = \frac{\mathbf{x_t}\mathbf{Q_t}^\top \odot \mathbf{x_0}\overline{\mathbf{Q}}_\mathbf{t-1}}{\mathbf{x_0}\overline{\mathbf{Q}}_\mathbf{t}\mathbf{x_t}^\top}\right). \tag{15}$$

As in (Austin et al., 2021), the neural network responsible for denoising $p_\theta(\tilde{\mathbf{x}}_\mathbf{0}|\mathbf{x_t}, g)$ is trained to predict the original data $\mathbf{x_0}$. During the reverse process, this predicted $\tilde{\mathbf{x}}_\mathbf{0}$ is used as a substitute for $\mathbf{x_0}$ to compute the posterior distribution:

$$\tilde{\pi}_\theta(\mathbf{x_{t-1}}|\mathbf{x_t}, g) = \sum_{\boldsymbol{x}} q(\mathbf{x_{t-1}}|\mathbf{x_t}, \tilde{\mathbf{x}}_\mathbf{0})\tilde{\pi}_\theta(\tilde{\mathbf{x}}_\mathbf{0}|\mathbf{x_t}, g) \tag{16}$$

B Neural Network Architecture

Following Sun & Yang (2023), we also utilize an anisotropic graph neural network with edge gating (Bresson & Laurent, 2018) for the backbone network of the diffusion model.

Consider h_i^ℓ and e_{ij}^ℓ as the features of node i and edge ij at layer ℓ, respectively. Additionally, let t represent the sinusoidal features (Vaswani et al., 2017) corresponding to the denoising timestep t. The propagation of features to the subsequent layer is performed using an anisotropic message-passing mechanism:

$$\hat{e}_{ij}^{\ell+1} = P^\ell e_{ij}^\ell + Q^\ell h_i^\ell + R^\ell h_j^\ell, \tag{17}$$
$$e_{ij}^{\ell+1} = e_{ij}^\ell + \text{MLP}_e(\text{BN}(\hat{e}_{ij}^{\ell+1})) + \text{MLP}_t(t), \tag{18}$$
$$h_i^{\ell+1} = h_i^\ell + \alpha(\text{BN}(U^\ell h_i^\ell + \sum_{j \in N_i} \sigma(\hat{e}_{ij}^{\ell+1}) \odot V^\ell h_j)), \tag{19}$$

where $U^\ell, V^\ell, P^\ell, Q^\ell, R^\ell \in \mathbb{R}^{d\times d}$ are learnable parameters for layer ℓ, α denotes the ReLU activation function (Krizhevsky & Hinton, 2010), BN stands for Batch Normalization (Ioffe & Szegedy, 2015), A signifies the aggregation function implemented as SUM pooling (Xu et al., 2019), σ is the sigmoid activation function, $\odot$ represents the Hadamard product, N_i indicates the neighbors of node i, and MLP$(\cdot)$ refers to a two-layer multi-layer perceptron.

For the Traveling Salesman Problem (TSP), the initial edge features e_{ij}^0 are derived from the corresponding values in x_t, and the initial node features h_i^0 are initialized using the nodes' sinusoidal features. In contrast, for the Maximum Independent Set (MIS) problem, e_{ij}^0 are initialized to zero, and h_i^0 are assigned values corresponding to x_t. We then apply a classification or regression head, with two neurons for classification and one neuron for regression, to the final embeddings of x_t (i.e., $\{e_{ij}\}$ for edges and $\{h_i\}$ for nodes) for discrete and continuous diffusion models, respectively.

C Experiment Details

C.1 Training Details for Supervised Learning

Since we leverage the trained checkpoints introduced by DIFUSCO (Sun & Yang, 2023) and T2T (Li et al., 2023), we adopt the datasets and training procedures mentioned in DIFUSCO as shown in Table 8. This approach ensures consistency with previous work and provides a solid foundation for our RL fine-tuning experiments.

Training Details	**TSP-50**	**TSP-100**	**TSP-500**	**TSP-1k**	**TSP-10k**	**SATLIB**	**ER-[700-800]**
Number of epochs	50	50	50	50	50	50	50
Number of instances	1502000	1502000	128000	64000	6400	49500	163840
Batch size	512	256	64	64	8	128	32
Learning rate schedule	Cosine schedule starting from 2e-4 and ending at 0						
Curriculum learning	No	No	Yes	Yes	Yes	No	No
Initialization	-	-	TSP-100	TSP-100	TSP-500	-	-

Table 8: DIFUSCO Training Details for different tasks

C.2 Training Details for RL fine-tuning

Most hyperparameters remain consistent in all experiments, with the primary variation in the number of training epochs as shown in Table 9. For RL fine-tuning starting from FastT2T within the CADO framework, as shown in Table 10, we use a relatively small number of epochs to verify the correctness and generalization of our framework.

C.3 Training Time Comparisons between RL fine-tuning and SL Learning

We compare the training time of our RL fine-tuning approach (CADO) against the standard SL training of DIFUSCO, as presented in Table 11. For a fair comparison, our RL fine-tuning process for each task was configured to use a similar number of training samples as the original SL training. For smaller-scale TSP instances (e.g., TSP-1k and below), where the original SL dataset is exceptionally large, CADO achieves its superior performance in significantly less training time. For tasks with smaller datasets, such as TSP-10k and

Table 9: RL Fine-Tuning Details for CADO for different CO tasks.

RL Fine-Tuning Details	**TSP**				**MIS**	
	100	**500**	**1k**	**10k**	**SAT**	**ER**
Number of epochs	3000	6000	6000	1000	5000	2500
Number of samples in each epoch	512					
Batch size	64					
Learning rate	1e-5					
Denoising step (Train)	10					
LoRA Rank	2					
Number of Selective layers	1					

Table 10: RL Fine-Tuning Details for different tasks from pre-trained model FastT2T (1,1).

RL Fine-Tuning Details	**TSP**			**MIS**	
	100	**500**	**1k**	**SAT**	**ER**
Number of epochs	1500	1500	1500	1500	1500
Number of samples in each epoch	512				
Batch size	64				
Learning rate	1e-5				
Denoising step (Train)	(1,1)				
LoRA Rank	2				
Number of Selective Layers	1				

MIS, the training times are comparable. Notably, across all evaluated tasks, CADO demonstrates substantial performance gains without incurring additional, and often with reduced, computational overhead for training.

Training Time (Hours)	**TSP-100**	**TSP-500**	**TSP-1k**	**TSP-10k**	**SATLIB**	**ER-[700-800]**
SL Learning	307	414	318.5	427	15	30
RL Fine-Tuning	5	41	148	434	30	16

Table 11: DIFUSCO Training Time Comparisons Between Various CO Tasks.

D Additional Experiments and Analysis

D.1 Comparison with Cost-aware diffusion Solvers

We hypothesize that direct objective alignment during training is fundamentally more effective than post-hoc cost-guidance applied during inference. To test this, we conduct a rigorous comparative study between CADO and leading heatmap-based solvers (DIFUSCO, T2T/FastT2T). The central challenge in comparing these methods is to disentangle the contribution of the core learning algorithm from the powerful search heuristics often used in concert. Therefore, we establish a controlled experimental testbed where auxiliary search techniques (e.g., Local Rewrite, 2-opt) are applied identically across all models. This ensures an apples-to-apples comparison, isolating the true impact of the underlying heatmap generation strategy. Moreover, we test the versatility of our approach by fine-tuning not only our base model (DIFUSCO) but also a pre-trained FastT2T model. This serves to demonstrate that CADO is not a model-specific trick, but a general framework for resolving the objective mismatch inherent in any SL-based heatmap solver.

D.2 Taxonomy of Search Techniques

To ensure a fair comparison, it is crucial to understand the roles of different search techniques employed by heatmap-based solvers. We categorize them based on their applicability and function:

- **Cost-guided denoising process (CS)**: This is a post-hoc inference technique specific to well-trained SL models like T2T. Similar to classifier guidance, it steers the generation process towards lower-cost solutions using a predefined energy function, $l(\boldsymbol{x}, c^\star|g)$, without any additional training:

$$\tilde{\pi}_\theta(\boldsymbol{x}|c^\star, g) \propto \tilde{\pi}_\theta(\boldsymbol{x}|g) l(\boldsymbol{x}, c^\star|g).$$

  Its primary limitation is being decoder-blind; it guides the heatmap based on a cost proxy, not the final decoded solution cost. Its effectiveness is also fundamentally constrained by the quality of the initial SL-trained model.

- **Local Rewrite (LR)**: A diffusion-specific iterative refinement method. It perturbs a solution by adding noise and then denoises it, a process that can discover better solutions. As a general technique, it can be applied to any diffusion-based solver, including DIFUSCO, T2T, and CADO.

- **2-opt**: A classic local search heuristic for the TSP. It iteratively swaps pairs of edges in a decoded tour to improve solution quality. While simple, it is highly effective when combined with a strong initial solution from a heatmap-based solver. As a problem-specific but model-agnostic heuristic, it can be applied to the output of any solver.

The key distinction for our analysis lies in their applicability. Local Rewrite and 2-opt are general-purpose search components that can be integrated into CADO and our baselines alike. In contrast, Cost-Guided Denoising is an approach fundamentally tied to the post-hoc correction paradigm of T2T while RL fine-tuning is tied to the CADO framework. Therefore, to precisely isolate the difference between T2T's post-hoc guidance and CADO's direct objective alignment, we conduct controlled experiments. In these experiments, the general search techniques (LR and 2-opt) are applied identically to both models (or disabled for both). This setup creates a direct comparison between the two core cost-awareness strategies: post-hoc Cost-Guided Search versus our end-to-end RL fine-tuning.

D.3 Controlled Experimental Settings for Fair Comparison

Since CADO shares its GNN architecture with prior works like DIFUSCO and T2T, the quality of the generated heatmap is fundamentally tied to the effectiveness of the neural network's training. However, the final performance of diffusion-based CO solvers is not determined by the heatmap alone. It is significantly influenced by various inference-time components, including the number of denoising steps and the use of auxiliary search techniques. Specifically, general-purpose heuristics such as Local Rewrite (LR) and 2-opt can substantially impact solution quality, often confounding the contribution of the core heatmap generation model. To dissect the true effect of each component and ensure a fair, rigorous comparison, we establish a controlled experimental testbed. We systematically evaluate all baselines under various settings, including configurations where these auxiliary techniques are either applied identically to all methods or disabled entirely. This controlled approach allows us to isolate the impact of our core contribution—RL-based objective alignment—from confounding factors. The detailed inference configurations for each algorithm are specified in Table 12.

D.4 Analysis for Simulation Results

Among heatmap-based CO solvers, several approaches also incorporate cost information with motivations similar to CADO. In this section, we highlight important baselines DIMES (Qiu et al., 2022), DIFUSCO (Sun & Yang, 2023), T2T (Li et al., 2023), and FastT2T (Li et al., 2024).

Table 12: Detailed inference configurations for diffusion-based solvers. This table outlines the specific parameters used for each method during inference. Initial Denoising Timesteps and Local Rewrite Timesteps define the core generation process. Number of Decoding refers to the total number of solution candidates generated. **Number of 2-opt (w/ 2-opt)** specifies the number of 2-opt applications in our main experiments, while **Number of 2-opt (w/o 2-opt)** is for the ablation study without the heuristic.

Algorithms	Methodology	Initial Generation iterations	Initial Denoising Timesteps	Local Rewrite iterations	Local Rewrite Denoising Timesteps	Total Denoising Timesteps	Number of Decoding	Number of 2-opt (w/o 2-opt)	Number of 2-opt (w/ 2-opt)
DIFUSCO	SL	1	50	0	0	50	1	0	1
CADO-L	SL + RL	1	20	0	0	20	1	0	1
T2T	SL+CS+LR	1	20	3	10	50	4	0	4
FastT2T (5,3)	SL+CS+LR	5	1	3	1	8	8	0	4
CADO	SL+RL+LR	1	20	3	10	50	4	0	4
FastT2T (1,0)	SL+CS	1	1	0	0	1	1	0	1
CADO + FastT2T (1,0)	SL+RL+LR	1	1	0	0	1	1	0	1
FastT2T (1,1)	SL+CS+LR	1	1	1	1	2	2	0	2
CADO + FastT2T (1,1)	SL+RL+LR	1	1	1	1	2	2	0	2

Table 13: Performance comparison of algorithms across various TSP and MIS problem instances. All algorithms are evaluated without the 2-opt heuristic.

Algorithms (w/o 2-opt)	Methodology	TSP-100		TSP-500		TSP-1k		TSP-10k		MIS-SAT		MIS-ER	
		Length ↓	Drop ↓	Length ↓	Drop↓	Length ↓	Drop↓	Length↓	Drop↓	Length↓	Drop↓	Length↓	Drop↓
DIFUSCO	SL	7.84	1.01%	18.11	9.41%	25.72	11.24%	98.15	36.75%	424.56	0.33%	36.55	18.53%
CADO-L	SL+RL	**7.77**	**0.19%**	**17.04**	**2.96%**	**24.55**	**6.17%**	**78.72**	**9.83%**	**425.27**	**0.16%**	**42.96**	**4.25%**
T2T	SL+CS+LR	7.77	0.18%	17.69	6.92%	25.39	9.83%	-	-	425.02	0.22%	39.56	11.83%
FastT2T (5,3)	SL+CS+LR	7.76	0.07%	17.45	5.45%	25.18	8.90%	-	-	-	-	40.61	9.52%
CADO	SL+RL+LR	**7.76**	**0.06%**	**16.77**	**1.35%**	**24.06**	**4.05%**	-	-	**425.43**	**0.12%**	**43.62**	**2.78%**
FastT2T (1,0)	SL+CS	7.91	1.99%	18.04	8.97%	26.68	15.41%	-	-	-	-	36.88	17.82%
CADO + FastT2T (1,0)	SL+RL+LR	**7.86**	**1.32%**	**17.69**	**6.87%**	**25.10**	**8.55%**	-	-	-	-	**39.82**	**11.25%**
FastT2T (1,1)	SL+CS+LR	7.78	0.49%	17.58	6.22%	25.94	12.2%	-	-	-	-	40.29	10.21%
CADO + FastT2T (1,1)	SL+RL+LR	**7.77**	**0.16%**	**17.23**	**4.11%**	**24.61**	**6.46%**	-	-	-	-	**41.16**	**8.28%**

D.5 Analysis of Heatmap Quality without 2-opt Heuristic

To isolate the intrinsic quality of the generated heatmaps, we first conduct a comparative analysis without the powerful search heuristic, 2-opt. This experiment directly evaluates the effectiveness of the underlying heatmap generation strategy of each model. The results, presented in Table 13, offer compelling evidence for the superiority of our approach.

D.5.1 CADO's RL Fine-Tuning Decisively Outperforms Baselines

Across all benchmarks, CADO demonstrates a significant performance advantage. Strikingly, even the ablated CADO-L—which forgoes Local Rewrite and thus requires only 40% of the computational budget of T2T—consistently outperforms both the fully-equipped T2T and the baseline DIFUSCO. This result underscores the profound impact of our direct objective alignment.

D.5.2 Direct Objective Alignment vs. Post-Hoc Guidance

The performance gap becomes even more pronounced in a direct comparison between CADO and T2T, which share identical settings (including Local Rewrite) and the same pre-trained model. On TSP-500/1k, CADO achieves drop of just 1.35%/4.05%. On the other hand, T2T's post-hoc cost guidance yields much larger gaps of 6.92%/9.83%. This wide disparity provides definitive proof of our central hypothesis: directly optimizing for the true, post-decoding cost via RL fine-tuning is fundamentally more effective than applying post-hoc corrections to a cost-blind heatmap.

D.5.3 Generalization and Robustness of the CADO Framework

To validate the general applicability of our framework, we fine-tuned a different pre-trained model, FastT2T. The results confirm that CADO consistently and substantially improves upon the original models, whether

Local Rewrite is used or not. This is particularly notable for the FastT2T(1,0) case, which uses a single denoising step and effectively acts as a standard regression-based heatmap-based solver. CADO's strong performance in this setting proves that our RL fine-tuning is a robust and principled method that works across different model architectures and configurations, not a trick specific to one setup.

D.6 Analysis of Heatmap Quality with 2-opt Heuristic

To assess the practical utility of our framework, we evaluate all methods in a more realistic scenario where a powerful post-hoc heuristic, 2-opt, is applied to the generated solutions. Table 14 shows that CADO consistently outperforms or remains highly competitive with all baselines, reaffirming its state-of-the-art performance. We observe that the performance gap between CADO and other methods is narrower compared to the experiments without 2-opt. This is an expected and insightful result. A strong local search heuristic like 2-opt can partially compensate for deficiencies in a less optimal initial heatmap, thus elevating the performance of all solvers. However, the final solution quality is still fundamentally anchored by the quality of the initial heatmap. CADO's superior performance, even after this normalization by 2-opt, decisively demonstrates that generating a better-aligned initial solution through our cost-aware framework is the most critical factor for achieving top-tier results. This confirms that CADO is not just theoretically sound but also practically effective in standard CO solver pipelines.

Table 14: Performance comparison of algorithms (w/ 2-opt) across various TSP instances. All algorithms are employed **with 2-opt**.

Algorithms (w/ 2-opt)	Methodology	TSP-100		TSP-500		TSP-1k		TSP-10k	
		Length ↓	Drop ↓	Length ↓	Drop↓	Length ↓	Drop↓	Length↓	Drop↓
DIFUSCO	SL+2-opt	7.78	0.41%	16.81	1.55%	23.55	1.86%	73.99	3.10%
CADO-L	SL+RL+2-opt	**7.77**	**0.12%**	**16.71**	**0.96%**	**23.44**	**1.39%**	**73.69**	**2.68%**
T2T	SL+CS+LR+2-opt	7.76	0.06%	16.68	0.83%	23.41	1.26%	-	-
FastT2T (5,3)	SL+CS+2-opt	7.76	**0.01%**	16.66	0.65%	23.35	0.99%	-	-
CADO	SL+RL+LR+2-opt	7.76	0.06%	**16.65**	**0.61%**	**23.32**	**0.88%**	-	-
FastT2T (1,0)	SL+CS+LR + 2-opt	7.77	0.18%	16.74	1.15%	26.68	15.4%	-	-
CADO + FastT2T (1,0)	SL+RL+LR +2-opt	7.77	0.14%	16.73	1.06%	23.45	1.43%	-	-
FastT2T (1,1)	SL+CS+LR + 2-opt	7.77	0.09%	16.74	1.12%	23.42	1.30%	-	-
CADO + FastT2T (1,1)	SL+RL+LR + 2-opt	**7.76**	**0.02%**	**16.67**	**0.70%**	**23.37**	**1.08%**	-	-

E TSPLIB experiment

To further demonstrate the robustness and consistency of our method on real-world problem instances, we provide a detailed per-instance performance breakdown on the TSPLIB benchmark. Table 15 covers instances with 50–200 nodes, while Table 16 covers larger instances from 200–1000 nodes. Across this diverse set of instances, CADO consistently achieves the lowest drop, outperforming all diffusion-based baselines. This confirms that CADO's superiority is not an artifact of averaging over a specific data distribution but a consistent advantage across various problem structures and scales.

Name	Optimal Len	AM		POMO		Sym-NCO		ELG		HierTSP		DIFUSCO		T2T		DEITSP		CADO	
		Length	Drop ↓	Length	Drop ↓	Length	Drop ↓	Length	Drop ↓	Length	Drop ↓	Length	Drop ↓	Length	Drop ↓	Length	Drop ↓	Length	Drop ↓
berlin52	7542.000	7856.426	4.169	7544.366	0.031	7544.662	0.035	7544.365	0.031	7544.662	0.035	7544.366	0.031	7544.366	0.031	7544.366	0.031	7544.365	0.031
bier127	118282.000	125270.101	5.908	123319.180	4.259	123993.359	4.829	122855.531	3.867	124093.656	4.913	119152.524	1.040	119050.160	0.649	119367.517	0.918	118760.281	0.404
ch130	6110.000	6304.420	3.182	6122.857	0.210	6118.715	0.143	6119.898	0.162	6157.908	0.784	6190.983	1.325	6122.493	0.204	6126.887	0.276	6114.782	0.078
ch150	6528.000	6827.244	4.584	6562.099	0.522	6567.454	0.604	6583.826	0.855	6578.063	0.767	6585.461	0.880	6580.099	0.798	6564.298	0.556	6555.628	0.423
eil101	629.000	647.832	2.994	640.596	1.844	640.212	1.782	643.840	2.359	642.830	2.199	641.458	1.981	642.587	2.155	644.122	2.404	640.264	1.790
eil51	426.000	432.935	1.628	431.953	1.397	431.953	1.397	430.746	1.114	429.484	0.818	431.271	1.237	429.484	0.818	433.943	1.747	428.981	0.699
eil76	538.000	548.717	1.992	544.369	1.184	544.652	1.236	549.433	2.125	547.020	1.677	545.048	1.310	556.769	3.489	544.369	1.184	544.369	1.183
kroA100	21282.000	22136.898	4.017	21396.438	0.538	21357.164	0.353	21307.422	0.119	21487.941	0.968	21285.443	0.016	21307.422	0.119	21307.422	0.119	21285.443	0.016
kroA150	26524.000	27527.668	3.784	26734.875	0.795	26890.738	1.383	26805.207	1.060	26995.578	1.778	26578.099	0.204	26525.031	0.004	26804.307	1.057	26525.031	0.003
kroA200	29368.000	31454.890	7.106	29984.789	2.100	30206.396	2.855	29831.221	1.577	30149.805	2.662	29583.978	0.735	30033.710	2.267	29543.848	0.599	29469.600	0.345
kroB100	22141.000	23279.490	5.142	22275.605	0.608	22374.285	1.054	22280.641	0.631	22275.350	0.607	22533.048	1.771	22645.401	2.278	22268.685	0.577	22508.477	1.659
kroB150	26130.000	26766.788	2.437	26635.195	1.933	26816.086	2.626	26374.766	0.937	26638.965	1.948	26284.696	0.592	26244.185	0.438	26319.820	0.726	26148.483	0.070
kroB200	29437.000	31951.214	8.541	30428.590	3.369	30563.463	3.827	29904.586	1.588	30551.854	3.787	30204.181	2.606	29841.325	1.374	29639.831	0.689	29518.668	0.277
kroC100	20749.000	20950.680	0.972	20832.773	0.404	20959.719	1.016	20770.041	0.101	20829.061	0.386	20773.073	0.116	20750.763	0.008	21293.943	2.626	20750.755	0.008
kroD100	21294.000	21872.558	2.717	21719.195	1.997	21635.557	1.604	21532.164	1.118	21772.988	2.249	21320.974	0.127	21294.291	0.001	21375.452	0.383	21294.290	0.001
kroE100	22068.000	22392.400	1.470	22380.355	1.415	22346.006	1.260	22237.137	0.766	22260.621	0.873	22372.583	1.380	22362.472	1.334	22424.825	1.631	22173.068	0.476
lin105	14379.000	14629.051	1.739	14494.633	0.804	14648.303	1.873	14467.038	0.612	14720.170	2.373	14432.139	0.370	14382.996	0.028	14382.996	0.028	14382.995	0.027
pr107	44303.000	46045.437	3.933	44897.246	1.341	45324.367	2.305	44960.422	1.484	44958.227	1.479	45551.263	2.818	44590.338	0.649	44519.916	0.490	44729.978	0.963
pr124	59030.000	61200.533	3.677	59091.836	0.105	59123.277	0.158	59181.652	0.257	59520.555	0.831	59814.535	1.329	59774.850	1.262	59607.740	0.979	59162.341	0.224
pr136	96772.000	101672.534	5.064	97485.609	0.737	97513.648	0.766	97733.406	0.993	98391.383	1.673	97664.229	0.922	96925.555	0.159	98097.238	1.369	96784.010	0.012
pr144	58537.000	63009.812	7.641	58828.539	0.498	59043.488	0.865	58859.398	0.551	58795.152	0.441	58853.339	0.540	59287.317	1.282	58604.905	0.116	58646.905	0.187
pr152	73682.000	79203.729	7.494	74440.711	1.030	76061.063	3.229	73720.609	0.052	74485.031	1.090	75613.977	2.622	74640.127	1.260	73683.641	0.002	74588.441	1.230
pr76	108159.000	109041.577	0.816	108159.438	0.000	108591.000	0.399	108444.047	0.264	108428.906	0.250	110019.494	1.720	109707.304	1.490	109086.647	0.926	109081.840	0.853
rat195	2323.000	2483.124	6.893	2558.470	10.136	2569.150	10.596	2400.750	3.348	2492.917	7.315	2392.573	2.995	2365.187	1.816	2355.277	1.196	2346.410	1.007
rat99	1211.000	1243.031	2.645	1273.635	5.172	1264.701	4.434	1248.142	3.067	1240.427	2.430	1220.098	0.751	1219.244	0.681	1219.244	0.681	1219.243	0.680
st70	675.000	686.725	1.737	677.110	0.313	677.110	0.313	677.110	0.313	677.110	0.313	677.642	0.391	677.194	0.325	677.110	0.313	677.109	0.312
Mean	31466.115	32703.968	3.934	31902.325	1.386	32069.482	1.917	31825.516	1.142	32025.602	1.778	31870.251	1.284	31750.494	0.903	31777.827	0.781	**31610.837**	**0.460**

Table 15: Comparison on TSPLIB instances with 50–200 nodes.

Name	Optimal Len	DIFUSCO		T2T		CADO	
		Length	Drop ↓	Length	Drop ↓	Length	Drop ↓
a280	2579.000	2714.408	5.25	2676.005	3.761	2589.557	0.409
d493	35002.000	35999.523	2.85	35831.093	2.369	35646.508	1.841
d657	48912.000	50127.103	2.484	50095.534	2.42	49693.430	1.598
fl417	11861.000	12284.844	3.573	12172.422	2.626	12082.369	1.866
p654	34643.000	35167.664	1.514	35011.017	1.062	34982.382	0.980
lin318	42029.000	43202.828	2.793	42465.811	1.039	42654.013	1.487
pr1002	259045.000	269491.268	4.033	266756.447	2.977	264527.769	2.117
pcb442	50778.000	52267.383	2.933	51418.603	1.262	51135.646	0.704
pr226	80369.000	81498.530	1.405	80863.979	0.616	80678.390	0.385
pr264	49135.000	49876.086	1.508	49648.489	1.045	49184.913	0.102
pr439	107217.000	111463.546	3.961	109562.481	2.188	108219.416	0.935
pr299	48191.000	49648.887	3.025	48806.939	1.278	48615.520	0.881
rat575	6773.000	6946.187	2.557	6893.903	1.785	6860.361	1.290
rat783	8806.000	9035.575	2.607	8986.024	2.044	8973.545	1.903
rd400	15281.000	15569.444	1.888	15434.598	1.005	15314.435	0.219
tsp225	3916.000	3988.991	1.864	3931.472	0.395	3923.511	0.192
ts225	126643.000	129143.181	1.974	128512.863	1.476	126725.437	0.065
u574	36905.000	37557.611	1.768	37414.204	1.38	37283.200	1.025
u724	41910.000	43019.140	2.646	42656.670	1.782	42504.571	1.419
Mean	53157.632	54684.326	2.665	54165.187	1.711	**53768.157**	**1.149**

Table 16: Comparison on TSPLIB instances with 200–1000 nodes.